Preprint typeset in JHEP style. - PAPER VERSION

Bicocca-F T-02-1
LAPTH-897/02
GEF-th-1/2002
hep-ph/0201281

Phenomenological study of charm photoproduction at HERA

Stefano Frixione*
Laboratoire d'Annecy-le-Vieux de Physique de Particules
Chemin de Bellevue, BP 110, 74941 Annecy-le-Vieux CEDEX, France

Paolo Nason
INFN, Sezione di Milano
Via Celoria 16, 20133 Milan, Italy

Abstract: We present predictions for single inclusive distributions of charmed mesons, relevant to the HERA experiments. Our results are based upon a computation that correctly incorporates mass effects up to the next-to-leading order level, and the resummation of transverse momentum logarithms up to next-to-leading-logarithmic level. We apply the same acceptance cuts as the H1 and Zeus experiments, and compare our results to their data. We perform a study of the sensitivity of our predictions on the charm mass, $\Lambda_{\rm QCD}$, factorization scale, renormalization scale, and fragmentation parameters.

Keywords: QCD, NLO Computations, Resummations, Hadron Colliders, Heavy Quark Physics.

*On leave of absence from INFN, Sez. di Genova, Italy

1 Introduction

In the present work we discuss phenomenological applications of the formalism presented in ref. [1], relevant to the production of heavy quarks in photon-hadron collisions. All technical details and theoretical motivations for the formalism are discussed there. In the formalism of ref. [1] one obtains a cross section which is accurate to $\mathcal{O}(\alpha_{\rm em}\alpha_{\rm s}^2)$ (that is, to the next-to-leading order level) and which, in the large $p_{\rm T}$ region, includes consistently all enhanced logarithmic terms of the form $\alpha_{\rm em}\alpha_{\rm s}(\alpha_{\rm s}\log p_{\rm T}/m)^i$ and $\alpha_{\rm em}\alpha_{\rm s}^2(\alpha_{\rm s}\log p_{\rm T}/m)^i$. Terms of order $\mathcal{O}(\alpha_{\rm em}\alpha_{\rm s}^3)$ with no logarithmic enhancement and terms of order $\alpha_{\rm em}\alpha_{\rm s}^3(\alpha_{\rm s}\log p_{\rm T}/m)^i$ are not included. Thus this approach improves both the fixed order (improperly called massive) and the resummed (improperly called massless) calculations.

Our starting point is the "matched" formula [1]

$$\text{FONLL} = \text{FO} \ + (\text{RS} \ - \ \text{FOM0}) \ \times G(m, p_{\rm T}) \ , \tag{1.1}$$

where FONLL stands for fixed-order plus next-to-leading logarithms, and

- FO is the fixed order, $\mathcal{O}(\alpha_{\rm em}\alpha_{\rm s}^2)$ result;
- RS is the resummed result, which includes all terms of the form $\alpha_{\rm em}\alpha_{\rm s}(\alpha_{\rm s}\log p_{\rm T}/m)^i$ and $\alpha_{\rm em}\alpha_{\rm s}^2(\alpha_{\rm s}\log p_{\rm T}/m)^i$, and neglects all terms suppressed by powers of the heavy quark mass m;
- FOM0 is the massless limit of FO, in the sense that all terms suppressed by powers of m are dropped, while logarithms of the mass are retained; thus FOM0 is the truncation of RS to order $\alpha_{\rm em}\alpha_{\rm s}^2$;
- $G(m, p_{\rm T})$ is an arbitrary dumping function, that must be regular in $p_{\rm T}$, and must approach 1 up to terms suppressed by powers of $m/p_{\rm T}$ at large $p_{\rm T}$; our standard choice is

$$G(m, p_{\rm T}) = \frac{p_{\rm T}^2}{p_{\rm T}^2 + c^2 m^2} \ , \tag{1.2}$$

  which for $c \neq 0$ dumps the RS $-$ FOM0 term in the small-$p_{\rm T}$ region.

We remind the reader that in the description given above the hadronic photon contribution is also included; the counting of the orders in $\alpha_{\rm em}$ and $\alpha_{\rm s}$ remains the same, provided one counts the parton density functions of the photon as carrying a $\alpha_{\rm em}/\alpha_{\rm s}$ factor. A more detailed discussion can be found in ref. [1].

This paper is organized as follows. In sect. 2 we specify our choices for the input parameters and the parton density functions (PDF's). Furthermore, the specific cuts that the Zeus and H1 collaborations use in their analyses are reported in this section. All the subsequent results will be based upon these choices.

In order to present meaningful phenomenological results, we need to consider a non-perturbative fragmentation function (NPFF) to account for the hadronization of the charm quark into a charmed hadron. The NPFF is the source of several uncertainties affecting the theoretical predictions. First of all, various forms of NPFF have been proposed in the literature (see ref. [2] and references therein for an updated review). Furthermore, while the application of NPFF is unambiguous in the large $p_{\rm T}$ region, at moderate and small $p_{\rm T}$ there are ambiguities, depending

upon the definition of the z variable (i.e., whether it refers to energy, momentum or "plus" component), and upon the choice of the frame in which it is defined. The impact of these ambiguities will be assessed in sect. 3.

Phenomenological results have also uncertainties depending upon the accuracy of the perturbative calculations (which we estimate by varying the renormalisation and factorisation scales), the allowed range in the value of the heavy quark mass and $\Lambda_{\rm QCD}$, and the choice of the PDF's. These uncertainties will be discussed in sect. 4.

The H1 [3] and the Zeus [4] collaborations have studied photoproduction of D^* mesons. The two experiments have different acceptances and apply different cuts to their data samples. In sect. 5 we compute the distributions presented in refs. [3, 4], implementing the same cuts that are used there.

In sect. 6 we give our conclusions.

2 Input parameters

All the results presented in this paper are relevant to photoproduction experiments where the photon arises from collinear radiation off an incoming electron. The radiation spectrum depends upon the cuts that are applied to define the photoproduction regime, which are typically Q^2 cuts. Further kinematic cuts are applied either to the the variable y (the ratio of the photon energy over the incoming electron energy) or, which is equivalent, to the variable W (the photon-proton center-of-mass energy). The cuts used in refs. [3, 4] are summarised in table 1. The H1

	$Q^2_{\rm max}$ (GeV^2)	$y_{\rm min}$	$y_{\rm max}$
Zeus	1	0.187	0.869
H1 ETAG44	0.009	0.02	0.32
H1 ETAG33	0.01	0.29	0.62

Table 1: Q^2 and y cuts used by H1 and Zeus in refs. [3, 4] to define a photoproduction event.

collaboration uses two different electron taggers, denoted as ETAG33 and ETAG44, and has thus two samples of photoproduction data. The electron and proton energies are fixed to 27.5 and 820 GeV respectively. The y range quoted for Zeus corresponds to $130 < W < 280$ GeV.

We compute the photon spectrum in the Weizsäcker-Williams approximation, in the improved form of ref. [5], which includes non-logarithmic terms enhanced at small y.

The central values and ranges of the physical parameters that we adopt in the present paper are summarised in table 2. The range in $\Lambda^{(5)}_{\rm QCD}$ reported in the table corresponds to the range $\alpha_{\rm s}(M_{\rm Z}) = 0.118 \pm 0.002$. We use the two-loop expression of $\alpha_{\rm s}$ throughout this work. The

	low	central	high
Proton PDF	CTEQ5M [6]		
Photon PDF	AFG [7]		
Charm quark mass m	1.2 GeV	1.5 GeV	1.8 GeV
$\Lambda^{(5)}_{\rm QCD}$	0.203	0.226	0.254

Table 2: Central values and ranges of the physical parameters adopted in this paper.

factorization and renormalization scales ($\mu_{\rm F}$ and $\mu_{\rm R}$) are set equal to $\mu_0/2$, μ_0 and $2\mu_0$, where $\mu_0 = \sqrt{p_{\rm T}^2 + m^2}$ is our default choice.

In table 3 we report the kinematic ranges of the cross section measurements used in the Zeus and H1 analyses. Notice that the D^* kinematics are described by $p_{\rm T}, \eta$ (pseudorapidity) in the Zeus analysis, and by $p_{\rm T}, y$ (rapidity) in the H1 analysis. Unfortunately, the same notation (y) is traditionally used to indicate the Weizsäcker-Williams variable, and the meson rapidity. However, no confusion should possibly arise. In what follows, y will always indicate the meson rapidity.

Zeus	$p_{\rm T}(D^*) > 2$ GeV	$\lvert\eta(D^*)\rvert < 1.5$
H1 ETAG44	$p_{\rm T}(D^*) > 2$ GeV	$\lvert y(D^*)\rvert < 1.5$
H1 ETAG33	$p_{\rm T}(D^*) > 2.5$ GeV	$\lvert y(D^*)\rvert < 1.5$

Table 3: Visible ranges for the H1 and Zeus analyses of refs. [3, 4].

3 Non-perturbative fragmentation function

We begin by discussing the ambiguities related to the implementation of the non-perturbative fragmentation in our calculation. A NPFF has to be convoluted with our full FONLL result. The convolution is unambiguously defined only at large transverse momenta (i.e. $p_{\rm T} \gg m$). One writes

$$\frac{d^3\sigma_H(k)}{d^3k} = \int d^3\hat{k}\; dz\, D_{\rm NP}(z) \frac{d^3\sigma_Q(\hat{k})}{d^3\hat{k}} \delta^3\left(\vec{k} - z\vec{\hat{k}}\right) , \tag{3.1}$$

where σ_H is the cross section for the production of the heavy-flavoured hadron[1] H with momentum k, and σ_Q is the cross section for the production of the heavy quark Q with momentum $\hat{k}$. $D_{\rm NP}(z)$ is the NPFF. In eq. (3.1) we assume that fragmentation scales the 3-momentum of the heavy quark. Different prescriptions are however possible: for example, one could assume that either $\hat{k}^0$ or $\hat{k}^0 + |\hat{k}|$ are scaled instead of $\vec{k}$. In all cases, it is assumed that $\vec{k}$ remains parallel to $\vec{\hat{k}}$, and the mass-shell condition is imposed to fix the remaining components of the meson momentum. Only in the large-$p_{\rm T}$ limit all these prescriptions coincide. Also, none of these definitions is boost invariant, since the condition of parallelism is frame dependent. Again, in the large-$p_{\rm T}$ limit boost invariance is recovered.

For the meson momentum k we expect the condition $k^2 = m_H^2$ to be satisfied. However, for the purpose of computing distributions, we can also use $k^2 = m^2$, and consider the difference to be just another ambiguity in our result. The reader may find unreasonable to adopt this second choice, since physically the on-shell condition of the meson H must apply. However, in the context of a perturbative QCD computation, setting $k^2 = m_H^2$ may appear unreasonable from other points of view. For example, if we produce a quark with maximal $p_{\rm T}$, and fragment it with $z = 1$, setting $k^2 = m_H^2$ would yield a meson with the same $p_{\rm T}$ but larger energy, which violates energy conservation. Similar examples can be given at small $p_{\rm T}$ and large rapidities. If we are far from the phase space boundaries, which is always our case, both choices are sensible, and their difference can be considered as an inherent uncertainty of the procedure.

[1] In what follows, we assume the hadron H to be a D^* meson, since the H1 and Zeus data that we use in this paper are relevant to D^* mesons.

In the following, we will always use the Peterson fragmentation function [8]

$$D_{\rm NP}(z) \propto \frac{1}{z}\left(1-\frac{1}{z}-\frac{\epsilon}{1-z}\right)^{-2} . \tag{3.2}$$

For the sake of the studies performed in the present section we will take it normalized to 1, i.e. we do not include the D^* production fraction. Although other choices of fragmentation function are possible, we only use eq. (3.2) because it is the most commonly adopted, and because recent phenomenological fits of the ϵ parameter, adequate to the present work, do exist [9, 10]. In refs. [2, 11] the reader will find studies of alternative forms.

Our default choices for the non-perturbative fragmentation are as follows:

- the z variable is defined by the equation $\vec{k} = z\vec{\hat{k}}$;
- the fragmentation frame (i.e., the frame where the equation $\vec{k} = z\vec{\hat{k}}$ holds) is the HERA laboratory frame;
- the mass shell condition is $k^2 = \hat{k}^2 = m^2$;
- the value of the Peterson parameter is $\epsilon = 0.02$.

We now study the effect of the ambiguities in the definition of the non-perturbative fragmentation on the pseudorapidity and on the transverse momentum distributions for the Zeus kinematic cuts. Our conclusions would not change had we used H1 cuts. We consider first the effect of the change of the fragmentation frame. We call scheme (A) our default choice of frame. We call scheme (B) the alternative choice of a longitudinally-boosted fragmentation frame, boosted with rapidity equal to the quark rapidity. Thus, in this frame the quark rapidity is zero. We notice that in scheme (A) the quark and the meson have the same pseudorapidity, while in scheme (B) they have the same rapidity.

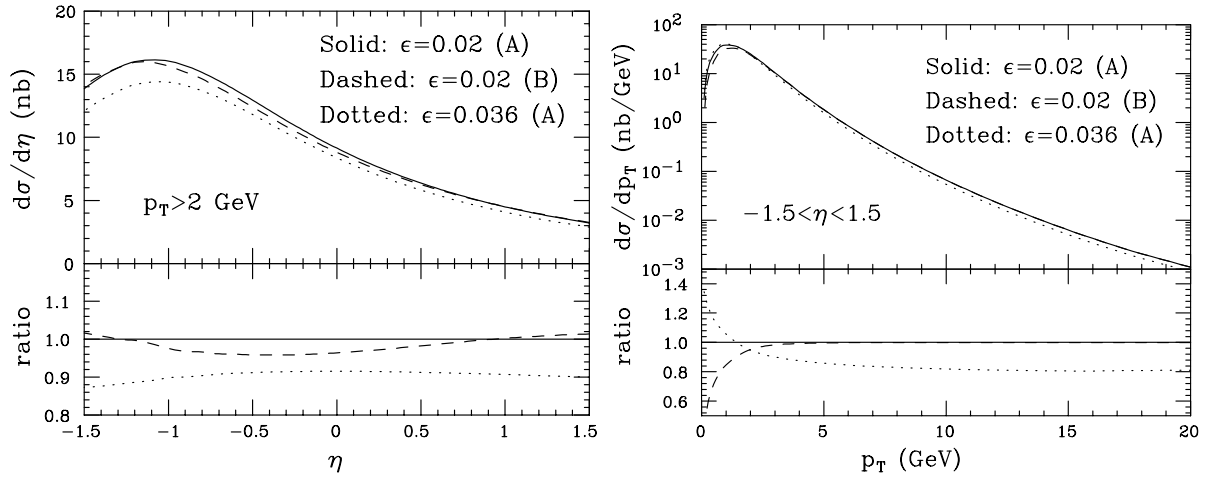

Figure 1: Fragmentation scheme and ϵ dependence of the pseudorapidity and transverse momentum distributions with Zeus cuts. The lower plots show the ratio of the variation over the default choice.

In figure 1 we show the difference in the pseudorapidity and transverse momentum distributions when using schemes (A) and (B). Furthermore, the effect of varying the value of the

Peterson parameter ϵ (in scheme (A)) is also shown. As we can see, the dependence on the fragmentation scheme is visible only for $p_{\rm T} < 3$ GeV. The rapidity distribution is mostly affected because of the relatively low $p_{\rm T}$ cut. The effect is generally modest, below 5% in the range of interest. When increasing ϵ, the $p_{\rm T}$ spectrum becomes softer. The spectrum with $\epsilon = 0.036$ is below the one with $\epsilon = 0.02$ for $p_{\rm T} > 1.5$ GeV; in the tail, the difference is of the order of 30%. As in the case of the fragmentation frame dependence, the behaviour of the $p_{\rm T}$ spectrum affects the η distribution through the $p_{\rm T}$ cut. When changing ϵ from 0.02 to 0.036, the η spectrum is almost unchanged in shape, and the normalisation decreases of about 10%.

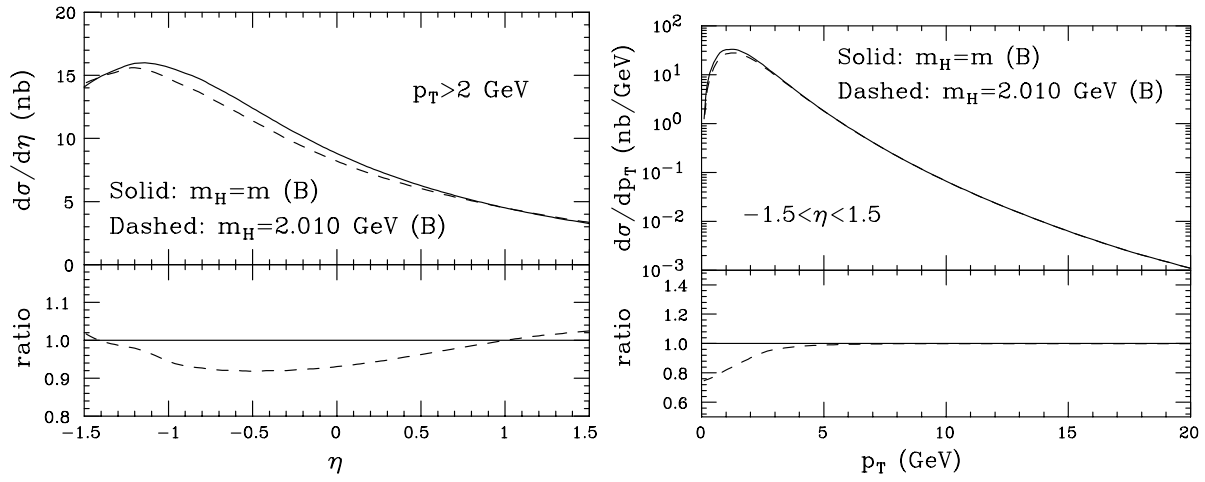

Figure 2: Effect of the on-mass-shell prescription in the pseudorapidity and transverse momentum distributions with Zeus cuts. The lower plots show the ratio of the variation over the default choice.

In figure 2 we show the difference in the pseudorapidity and transverse momentum distributions when using the mass of the quark (our default choice) for the on-mass-shell condition, as opposed to the mass of the D^* meson ($m_{D^*} = 2.010$ GeV). The comparison is performed in scheme (B), since in scheme (A) there is no difference in $p_{\rm T}$ and η for the two mass choices. The effect is only visible below $p_{\rm T} = 5$ GeV. In the case of HERA experiments, only $p_{\rm T} > 2$ GeV is relevant; in this region, the variation is below 10%. Furthermore, larger relative variations are observed only for very small $p_{\rm T}$, where the differential cross section is actually smaller in absolute value.

4 Dependence upon input parameters

We now turn to the study of the sensitivity of our result to the chosen range of parameters. We begin by showing in fig. 3 the sensitivity to the choice of $\Lambda_{\rm QCD}$. As we can see the sensitivity is quite small, below 10%. This is a consequence of the fact that the allowed range for $\Lambda_{\rm QCD}$ has become fairly narrow at present.

We do not include in our study the correlation of $\Lambda_{\rm QCD}$ with the parton densities, since PDF sets with flavour matching conditions consistent with our scheme that allow for $\Lambda_{\rm QCD}$ variation are not available at present. For the same reason, we do not include a study of the uncertainty due to the choice of the PDF set. In general, the inclusion of such an uncertainty is a highly non trivial problem, and it is far from having a satisfactory solution at present. However, it

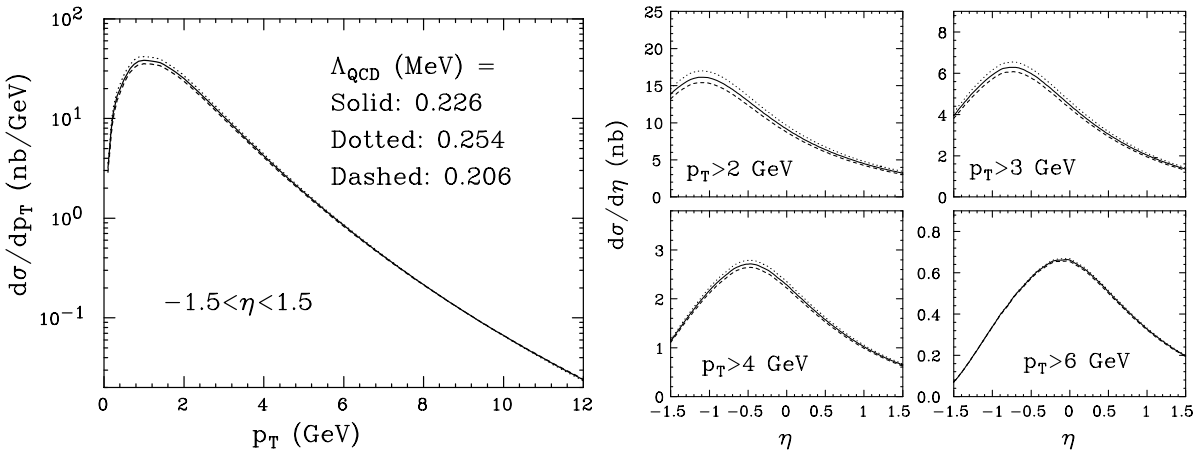

Figure 3: Sensitivity of the transverse momentum and pseudorapidity distributions to the choice of $\Lambda_{\rm QCD}$.

must be said that current PDF sets have rather similar gluon densities in the x region probed by charm production at HERA; therefore, we do not expect the PDF dependence to be a major source of uncertainty in our case.

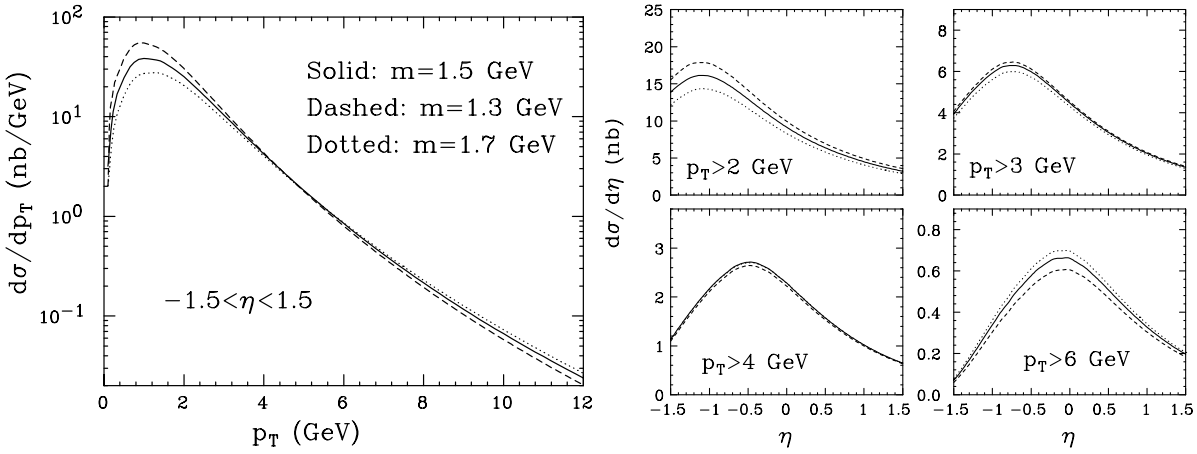

Figure 4: Sensitivity of the transverse momentum and pseudorapidity distributions to the choice of the charm mass.

The mass sensitivity is shown in fig. 4. The cross section is most sensitive to the mass value for $p_{\rm T}$ of the order of 1 GeV. In the visible range ($p_{\rm T} > 2$ GeV) the sensitivity is modest, of the order of 10%.

It has to be pointed out that our study of mass sensitivity is somewhat incomplete. In fact, we do not have the possibility of varying the charm mass in the evolution of the parton densities. Studies performed in the hadroproduction case have indicated that these effects are small.

The renormalization and factorization scale dependences are displayed in figures 5 and 6 respectively. The factorization scale choice has little impact on our results, except for small transverse momenta. In particular, when $\mu_{\rm F} = \mu_0/2$, at small $p_{\rm T}$ the cross section becomes unphysical, since it depends upon the parton densities at low scales, a region where current

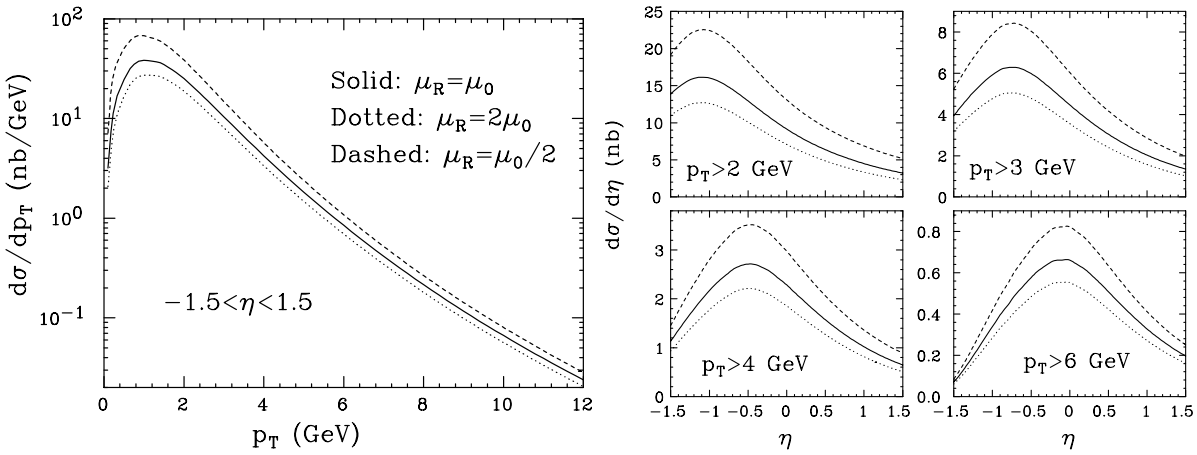

Figure 5: Sensitivity of the transverse momentum and pseudorapidity distributions to the choice of the renormalization scale.

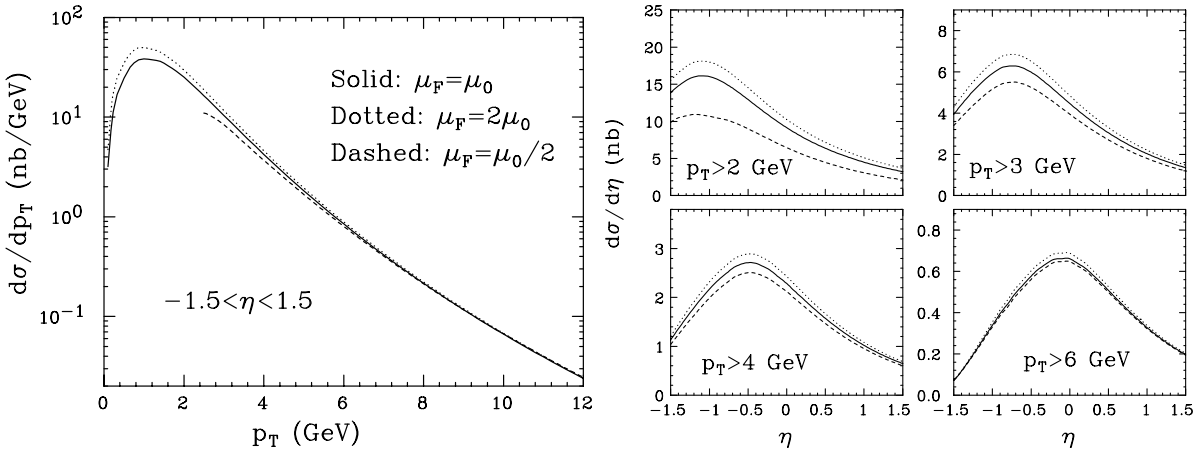

Figure 6: Sensitivity of the transverse momentum and pseudorapidity distributions to the choice of the factorization scale.

parametrizations are unreliable. We simply truncate the theoretical predictions at small transverse momenta in this case. The renormalization scale dependence is instead sizable in the whole production range. Since no data are available for $p_T < 2$ GeV, the inspection of figures 3-6 allows us to conclude that the renormalization scale dependence is the largest source of uncertainty when comparing the theoretical results to the data.

5 Comparison with data

In this section, we compare the theoretical predictions, obtained with our FONLL formalism, with the data relevant to D^* production, presented by the H1 and Zeus collaborations in refs. [3, 4]. For the sake of this comparison, we now need to multiply the NPFF of eq. (3.2) by a factor of 23.5 %, to take into account the $c \to D^*$ fraction [12]. Furthermore, we multiply by a factor of 2 in order to get the $D^{*+} + D^{*-}$ cross section, which is what the experiments quote in refs. [3, 4]. H1 data are presented in ref. [3] as γp cross sections, obtained by dividing the

measured photoproduction ep cross sections by the Weizsäcker-Williams flux; here, we quote the data as ep cross sections.

In QCD, it is very often the case that the theoretical uncertainties are larger than the experimental errors. Thus, an estimate of these uncertainties is mandatory for a meaningful comparison with the data. Usually, one takes the maximum and minimum values of the theoretical predictions, in the allowed range of the input parameters, as an estimate of the upper and lower theoretical errors. In our case, since the computation is numerically intensive, this procedure is too time consuming. We have thus adopted the following procedure. We construct an error band for our predictions by adding linearly all the variations that we have discussed in the previous section. In other words, for each parameter x (mass, $\Lambda_{\rm QCD}$, $\mu_{\rm R}$, $\mu_{\rm F}$) that has central value x_0 and upper and lower values x_h and x_l respectively, we define an upper and lower error

$$\delta_x^{\rm up} = \max[\sigma(x_0), \sigma(x_h), \sigma(x_l)] - \sigma(x_0)\,, \tag{5.1}$$

$$\delta_x^{\rm down} = \sigma(x_0) - \min[\sigma(x_0), \sigma(x_h), \sigma(x_l)]\,, \tag{5.2}$$

with all the other parameters in the cross section kept fixed to their central values. We then define our upper (lower) end of the band as the central cross section plus (minus) the sum of all upper (lower) errors. By interpreting eqs. (5.1) and (5.2) as true errors affecting the theoretical predictions, we could have also adopted the strategy of adding them quadratically. We refrain from doing this, since it is actually very doubtful that they obey a Gaussian law. However, it must be stressed that, in practice, the quadratic sum differs only by a tiny amount from the linear one, since they are both dominated by the effect due to the renormalization scale, as discussed in the previous section.

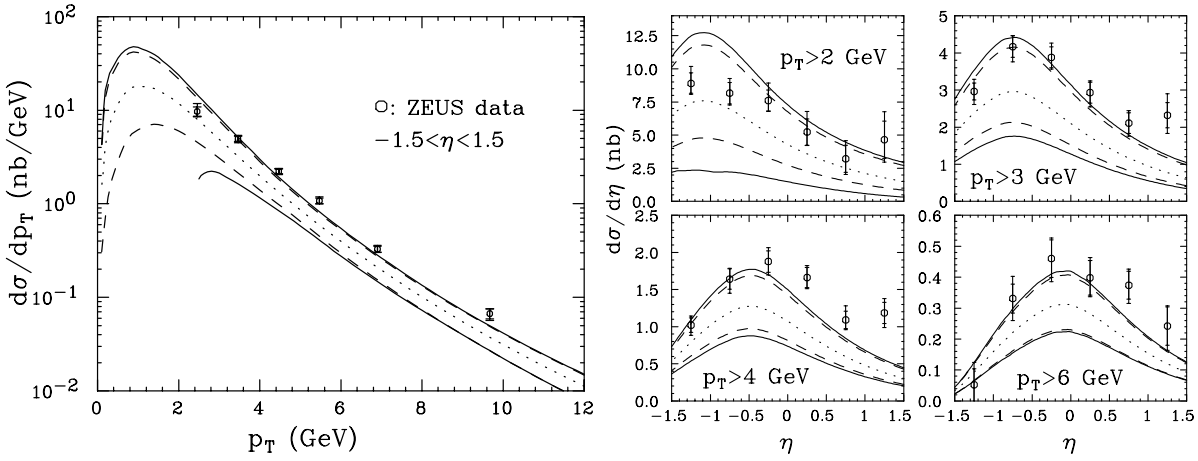

Figure 7: Comparison of Zeus data with the theoretical predictions. The dotted curve is the central value, the band included between the solid curves is obtained by adding linearly the uncertainties, the dashed band does not include the factorization scale uncertainty.

The lower error due to the factorization scale dependence is undefined for small momenta. Thus, the lower end of the band is undefined for low momenta if the factorization scale dependence is included in the error. We therefore present one band that includes the factorization scale error, and one band that does not include it. Since the factorization scale dependence is in general rather small, the difference between the two bands is non-negligible only in the small-$p_{\rm T}$ region, basically outside the region visible to experiments.

We begin with Zeus data from ref. [4], for which we present a comparison with our FONLL predictions in fig. 7. As often stated in the literature, the data lie above the theoretical predictions obtained with the default choice of parameters. On the other hand, we see that the data are marginally consistent with our upper band. However, the data seem to indicate a $p_{\rm T}$ spectrum harder than that suggested by QCD. As far as the pseudorapidity distribution is concerned, QCD appears to do a decent job, except in the positive-η region. The rightmost data points, however, are by far the ones affected by the largest errors.

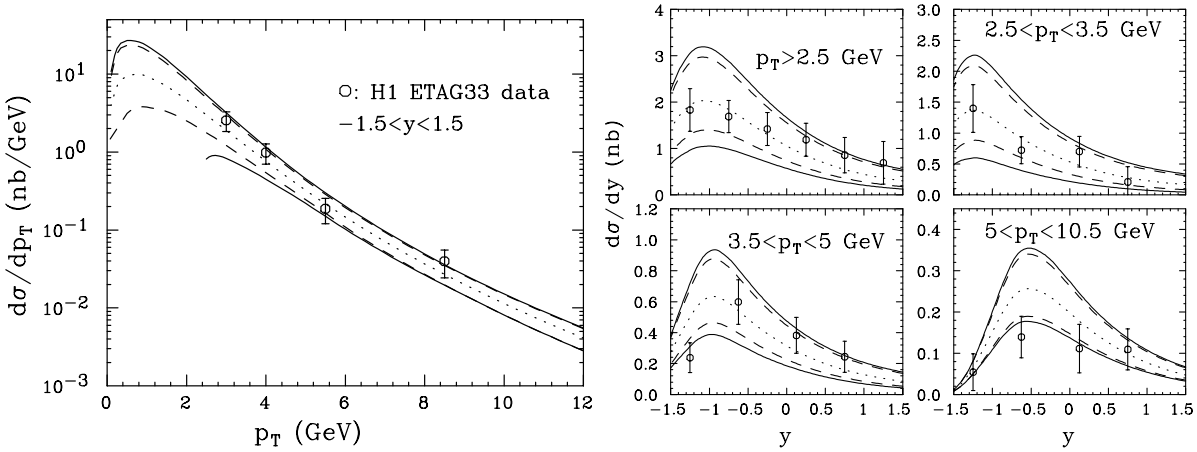

Figure 8: As in fig. 7, for the H1 ETAG33 data.

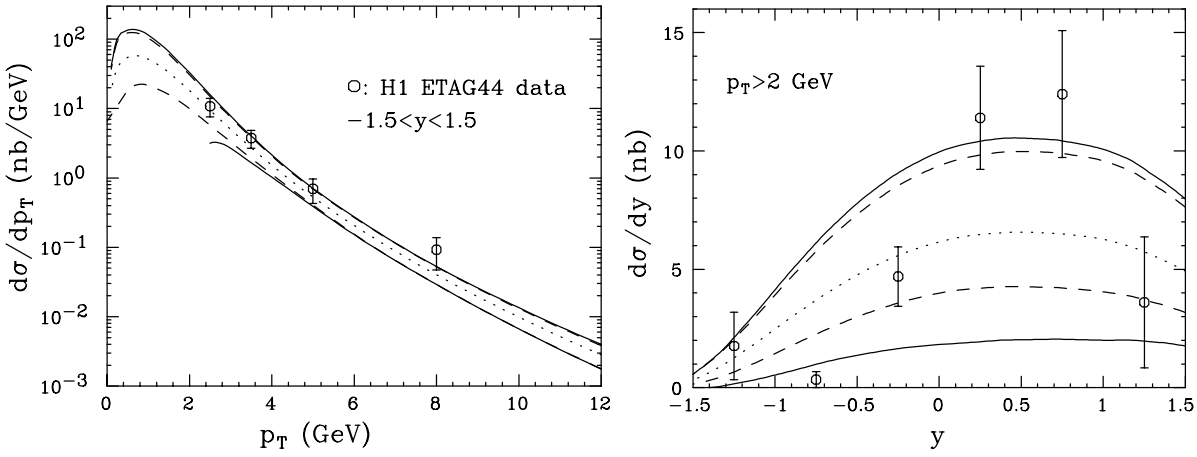

Figure 9: As in fig. 7, for the H1 ETAG44 data.

The data from H1 are compared to our calculations in fig. 8, for the ETAG33 sample, and in fig. 9, for the ETAG44 sample. In the case of the y spectra relevant to the cuts $2.5 < p_{\rm T} < 3.5$ GeV, $3.5 < p_{\rm T} < 5$ GeV, and $5 < p_{\rm T} < 10.5$ GeV, we multiply the data by the width of the $p_{\rm T}$ bin size, since they are originally quoted in ref. [3] as $d\sigma/dydp_{\rm T}$ cross sections. The $p_{\rm T}$ spectra are perfectly described by our FONLL predictions; all the data points are consistent with the default predictions within one standard deviation, with the marginal exception of the largest-$p_{\rm T}$ point in the ETAG44 sample. Shape-wise, the y spectrum of the ETAG33 sample

is also statistically compatible with QCD predictions; the same can be said for the ETAG44 sample, although in this case the statistical significance is clearly lower.

In order to assess more quantitatively the size of the agreement (or disagreement) between theory and data, we now present a comparison between the two in a different form. We compute, for each data point, the corresponding FONLL default prediction, and we consider the ratio data/FONLL. The results are presented as open points in fig. 10 for the $p_{\rm T}$ spectra, and in figs. 11 and 12 for the η and y spectra. The figures also display bands, whose pattern is identical to that of the bands in figs. 7–9. The current bands are in fact obtained by computing the ratios of FONLL bands over FONLL default predictions.

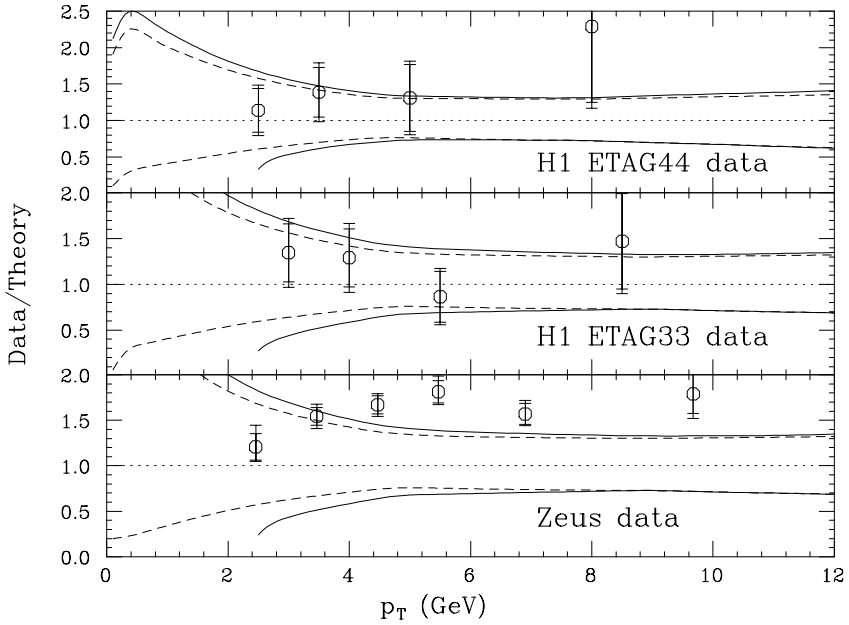

Figure 10: Open points: ratio of data over FONLL default predictions, for transverse momentum spectra measured by Zeus and H1. Solid and dashed curves are the ratios of FONLL bands over FONLL default predictions.

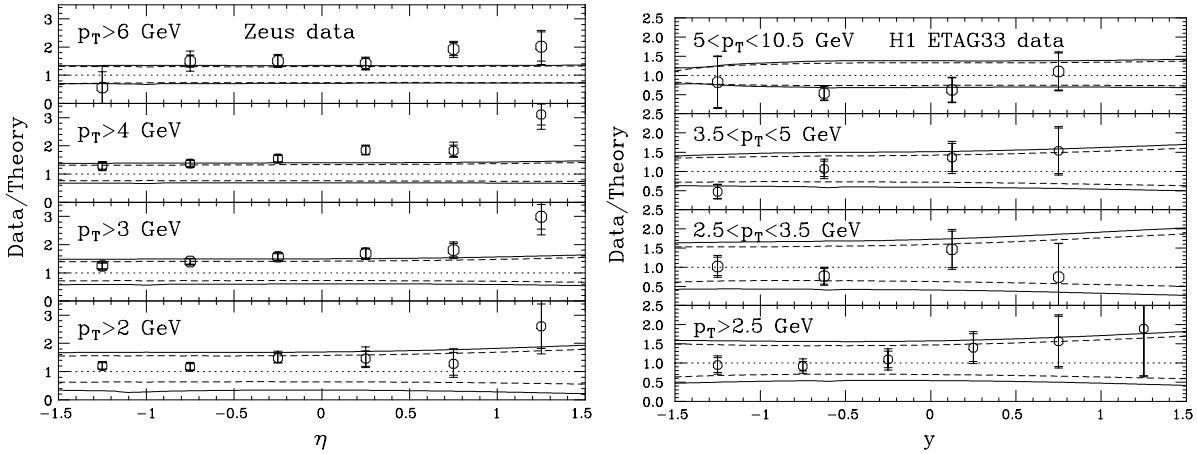

Figure 11: As in fig. 10, for Zeus η distribution (left) and H1 ETAG33 y distribution (right).

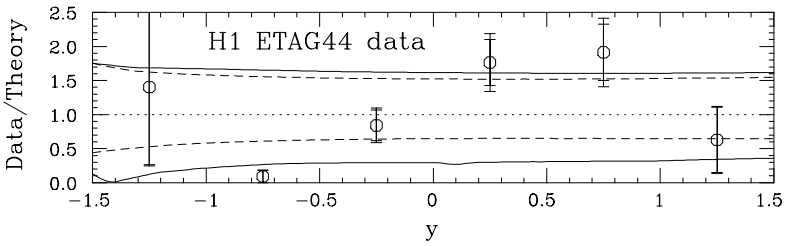

Figure 12: As in fig. 10, for H1 ETAG44 y distribution.

The lower inset of fig. 10 clearly shows that four (out of six) data points relevant to the $p_{\rm T}$ spectrum measured by Zeus are more than one standard deviation away from the upper end of the theoretical band. The measured spectrum appears to be harder than predicted; however, the effect is probably statistically not significant in the case in which the lowest-$p_{\rm T}$ measurement is excluded from the data sample. All but the lowest-$p_{\rm T}$ point are more than 50% away from the default prediction, but still within a factor of 2. On the other hand, there appears to be a nice agreement between H1 ETAG33 and FONLL predictions; ETAG44 data are also reasonably reproduced, but there the large errors prevent from reaching firm conclusions.

The case of the η and y spectra is dealt with in figs. 11 and 12. As far as the Zeus data are concerned, fig. 11 confirms the trend already visible in fig. 7: for all the $p_{\rm T}$ cuts, the measured distributions are more enhanced in the positive-η region than FONLL predicts. This trend is however weaker if the rightmost data points, those affected by the largest errors, are excluded from the data sample. Also, by excluding these points all data are within a factor of 2 from the default theory result. In general, most of the experimental results lie inside the theoretical uncertainty band. As already in the case of the $p_{\rm T}$ spectrum, H1 data do not suggest any statistically-significant deviation from FONLL predictions.

From this study, we see that Zeus and H1 data compare differently to FONLL predictions, the former displaying some disagreements with theory that are not present in the latter. It is difficult to understand whether the two data sets are compatible within errors, since the two experiments have different visible regions, and use different observables (Zeus use η, H1 use y).

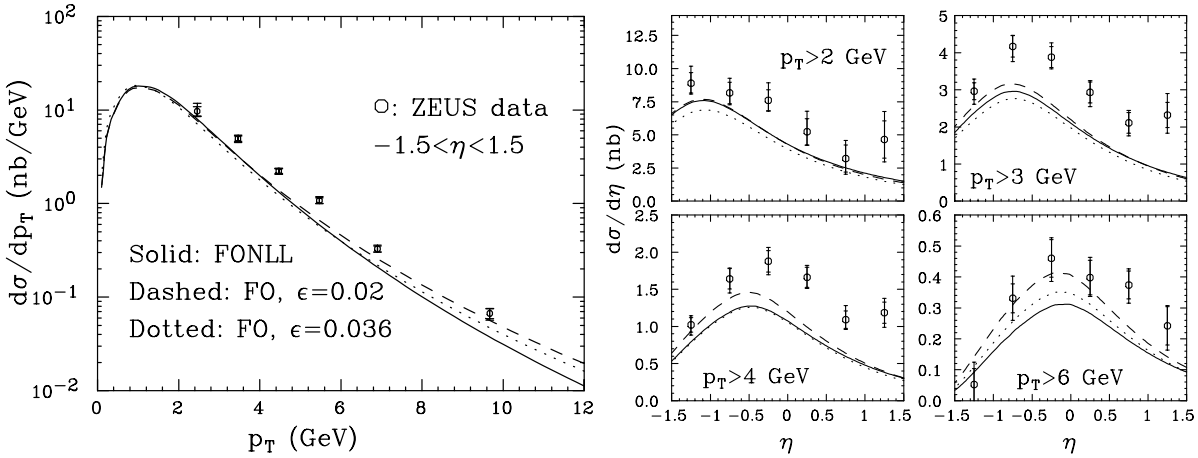

Figure 13: Comparison of Zeus data with the theoretical predictions. The solid curve is FONLL, the dashed curve is FO (at NLO).

The error bands presented in this section do not include any of the uncertainties relevant to the non-perturbative fragmentation discussed in sect. 3. This appears to be justified for the choice of the fragmentation frame and of the on-mass-shell condition, given the size of the effects induced. The choice of the ϵ parameter is phenomenologically more relevant, since it can give an up to 20% effect on the $p_{\rm T}$ spectrum. However, it has to be kept in mind that ϵ is not a physical quantity; in particular, its value crucially depends upon the scheme in which the hard cross section, which is convoluted with the NPFF, is defined. According to ref. [10], $\epsilon = 0.02$ is the value to be used in the case of a FONLL computation in order to obtain a meaningful comparison with data. The study of sect. 3 simply suggests that a larger (smaller) ϵ value gives a softer (harder) $p_{\rm T}$ spectrum. Thus, the comparison of FONLL predictions to Zeus data appears to imply the necessity of an even smaller ϵ value than the LEP data fit performed in ref. [10] suggests. On the other hand, H1 data appear to be consistent with $\epsilon = 0.02$.

It is interesting to compare the FONLL and FO calculations. The two predictions are displayed in fig. 13 for the Zeus cuts. FONLL results are obtained with the default parameters. We show two sets of FO curves. One set (dotted curves) is obtained with default parameters except for the value of ϵ, set equal to 0.036. This is in fact the value that gives the best fit to e^+e^- D^* production data when a FO calculation is used [10]. The other set (dashed curves) has $\epsilon = 0.02$. We include it in order to emphasise, in comparison to the FONLL result, the effect of the large-log resummation, which is only present in the latter. As expected (see sect. 1 and ref. [1]), FONLL and FO predictions (with the same ϵ) coincide at small $p_{\rm T}$'s; the difference between the two becomes visible for $p_{\rm T} > 4$ GeV. Where the two predictions differ, FONLL must be considered superior. Notice that although none of the two predictions agree well with data, the shape is better described by the FONLL calculation. We interpret this result as evidence of the onset of resummation effects in the data. In fact, the FO result requires larger value of ϵ in order to compensate for the lack of resummation effects.

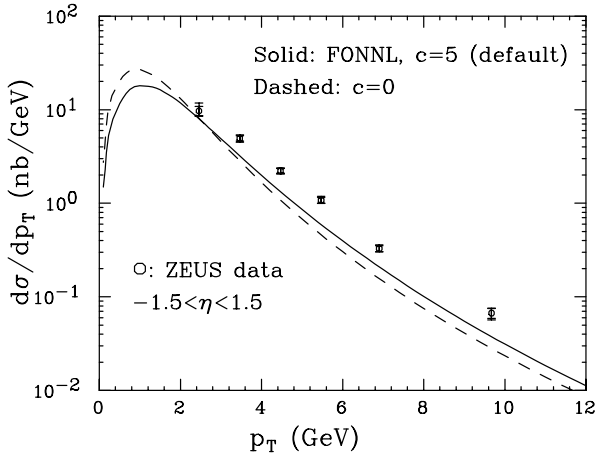

Figure 14: Comparison of the $c = 5$ and $c = 0$ choice.

We do not present here RS predictions, since we believe that in most of the visible range the transverse momentum is simply too small for them to apply. The RS result is below our FONLL result by 20% to 30% in the region $4 < p_{\rm T} < 20$ GeV, the difference becoming smaller as $p_{\rm T}$ increases. This difference is due to our choice of the c parameter that appears in eq. (1.2), which we fixed to 5 on the basis of the fact that, in the hadronic component of the cross section at the NLO level, the massless limit of the cross section is a good approximation of the massive cross section only for $p_{\rm T} \gtrsim 5m$ [1, 13]. We show our prediction for the extreme choice $c = 0$ in fig. 14. The $c = 0$ choice has a softer spectrum, and it undershoots our default choice by at most 25% in the large $p_{\rm T}$ region.

The definition of a photoproduction event in Zeus and H1 is slightly different, since the allowed photon virtuality is much smaller in H1. Thus, one is tempted to ask whether the differences of H1 and Zeus data compared to QCD calculations are due to the fact that Zeus

is not completely in the photoproduction regime. The Weizsäcker-Williams approximation is valid up to non-factorizable terms of order [5]

$$\delta = \frac{Q^2_{\rm max}}{S_{\rm min}} = \frac{Q^2_{\rm max}}{4m^2} \, , \tag{5.3}$$

which yields $\delta \approx 0.1$ for Zeus, and $\delta \approx 0.001$ for H1. This does not mean that one can expect non-factorizable terms of order 10% in the Zeus case, since the leading Weizsäcker-Williams term is logarithmically enhanced by a factor of $\log 4m^2/m_e^2 \approx 17$. Thus, one expects non-factorizable terms to be of the order of a percent in the Zeus case, and one hundred times smaller in the H1 case. It is thus unlikely that they could be the cause of the differences. A direct comparison of Zeus and H1 data, using the same kinematical cuts, would thus be useful to understand whether the two data sets are consistent among each other.

6 Conclusions

In this paper, we have presented comparisons between theoretical FONLL predictions and data relevant to the photoproduction of D^* mesons, as measured at HERA by the Zeus and H1 collaborations. We have studied the uncertainties affecting QCD predictions, and thus estimated the largest possible range for theoretical cross sections. Generally speaking, the agreement between theory and data is acceptable, after a tuning of the input parameters. While H1 data do not display any significant discrepancies with FONLL predictions, Zeus data seem to suggest a harder transverse momentum spectrum, and an excess towards the positive-pseudorapidity region. A detailed comparison between the two sets of data is not possible due to the different observables and visible regions used by the two experiments.

Having established that QCD does a reasonable job in describing charm data, it is interesting to notice that Zeus and H1 collaborations have now presented several results on bottom production [14, 15, 16, 17], that compare much worse to QCD predictions than analogous charm results. Since QCD expectations for charm agree reasonably with data, one would expect even better agreement for the bottom quark, because of the larger mass. It is thus unlikely that the bottom excess may be attributed to a failure of QCD predictions.

Acknowledgments

We wish to thank the CERN theory division for kind hospitality during the preparation of this work. We also would like to thank M. Cacciari, L. Gladilin and C. Grab for useful discussions.

References

[1] M. Cacciari, S. Frixione, and P. Nason, *The $p_{\rm T}$ spectrum in heavy-flavor photoproduction*, *JHEP* **03** (2001) 006, [hep-ph/0102134].

[2] O. Biebel, P. Nason, and B. R. Webber, *Jet fragmentation in e^+e^- annihilation*, hep-ph/0109282.

[3] **H1** Collaboration, C. Adloff *et. al.*, *Measurement of D^* meson cross sections at HERA and determination of the gluon density in the proton using NLO QCD*, *Nucl. Phys.* **B545** (1999) 21–44, [hep-ex/9812023].

[4] **ZEUS** Collaboration, J. Breitweg *et. al.*, *Measurement of inclusive D^{*+-} and associated dijet cross sections in photoproduction at HERA*, *Eur. Phys. J.* **C6** (1999) 67–83, [hep-ex/9807008].

[5] S. Frixione, M. L. Mangano, P. Nason, and G. Ridolfi, *Improving the Weizsäcker-Williams approximation in electron–proton collisions*, *Phys. Lett.* **B319** (1993) 339–345, [hep-ph/9310350].

[6] **CTEQ** Collaboration, H. L. Lai *et. al.*, *Global QCD analysis of parton structure of the nucleon: CTEQ5 parton distributions*, *Eur. Phys. J.* **C12** (2000) 375–392, [http://arXiv.org/abs/hep-ph/9903282].

[7] P. Aurenche, J. P. Guillet, and M. Fontannaz, *Parton distributions in the photon*, *Z. Phys.* **C64** (1994) 621–630, [hep-ph/9406382].

[8] C. Peterson, D. Schlatter, I. Schmitt, and P. M. Zerwas, *Scaling violations in inclusive e^+e^- annihilation spectra*, *Phys. Rev.* **D27** (1983) 105.

[9] M. Cacciari and M. Greco, *D^* production from e^+e^- to ep collisions in NLO QCD*, *Phys. Rev.* **D55** (1997) 7134–7143, [hep-ph/9702389].

[10] P. Nason and C. Oleari, *A phenomenological study of heavy-quark fragmentation functions in e^+e^- annihilation*, *Nucl. Phys.* **B565** (2000) 245–266, [hep-ph/9903541].

[11] P. Nason *et. al.*, *Bottom production*, hep-ph/0003142.

[12] L. Gladilin, *Charm hadron production fractions*, hep-ex/9912064.

[13] M. Cacciari, M. Greco, and P. Nason, *The p_{T} spectrum in heavy-flavour hadroproduction*, *JHEP* **05** (1998) 007, [hep-ph/9803400].

[14] **H1** Collaboration, C. Adloff *et. al.*, *Measurement of open beauty production at HERA*, *Phys. Lett.* **B467** (1999) 156–164, [hep-ex/9909029]. Erratum-ibid. **B 518**, 331-332, (2001).

[15] **ZEUS** Collaboration, J. Breitweg *et. al.*, *Measurement of open beauty production in photoproduction at HERA*, *Eur. Phys. J.* **C18** (2001) 625–637, [hep-ex/0011081].

[16] **H1** Collaboration, C. Adloff *et. al.*, *Measurement of the beauty production cross section at HERA using lifetime information*, ICHEP 2000, 30th International conf. on HEP, Osaka, Japan, July 2000.

[17] **H1** Collaboration, C. Adloff *et. al.*, *Beauty production in Deep Inelastic Scattering*, abstract 807 at Moriond-QCD 2001, March 2001.